Analysis and Reduction on In-Band RCS of Fabry-Perot Antennas

LEI GAN[1], WEN JIANG [1], (Member, IEEE), QIANG CHEN [1], (Senior Member, IEEE), XIAOQIU LI[2], AND ZHIPENG ZHOU[2]

[1]Science and Technology on Antenna and Microwave Laboratory, Xidian University, Xi'an 710071, China
[2]Nanjing Research Institute of Electronics Technology, Nanjing 210039, China

Corresponding author: Wen Jiang (jw13@vip.qq.com)

ABSTRACT In this article, a method is proposed to reduce the in-band radar cross section (RCS) of the high-gain Fabry-Perot antenna (FPA) based on the cancellation between the antenna mode RCS (AM-RCS) and structural mode RCS (SM-RCS). The ports of the two back-fed microstrip array antennas are connected to form the partial reflective surface (PRS) with a high reflectivity. The phase delay line (PDL) is proposed to control the AM-RCS to cancel out the SM-RCS. The AM-RCS is used to further reduce the in-band RCS of the low RCS high-gain FPA instead of being eliminated by the matched load. The measured results show that the FPA has a great impedance matching within the band of 9.8-11.2 GHz, and the maximum realized gain of the FPA reaches 10.7 dBi. The simulated bistatic RCS of the FPA is less than −14 dBsm within ±90 degrees angle domain at the center frequency. The minimum monostatic RCS of the proposed FPA is reduced by 17.9 dB compared with the reference FPA. Furthermore, this article provides a design basis for the feed line length of the FPA from the perspective of scattering performance.

INDEX TERMS Antenna mode radar cross section (AM-RCS), fabry-perot antenna (FPA), dividing scattering field, radar cross section (RCS).

I. INTRODUCTION

Antenna stealth technologies aim to lower the probability of antennas being detected by radar through reducing their RCS. As we all know, the RCS of antennas consists of two components: antenna mode radar cross section (AM-RCS) and structural mode RCS (SM-RCS) [1]. The AM-RCS originates from the reradiation of antennas under an incident plane wave, which is related to the radiation performance and loads of the antennas. The SM-RCS is the remainder of the total RCS to remove the AM-RCS. In the ordinary way antennas are installed on a large metal carrier, the SM-RCS much larger than the AM-RCS is the main reduction target.

The principle of RCS reduction is deflecting the scattering energy out of the threat angle or converting it into heat. Two typical methods are shaping [2] and coating radar absorbing materials [3]. The former has a limited effect and may degrade the radiation performance of the antenna, while the latter has a high cost. In recent years, antennas RCS reduction technologies based on metamaterials emerge in endlessly. The frequency selective surface (FSS) [4]–[6] and metamaterial absorber (MA) [7]–[9] can manipulate the magnitude

of scattering waves. The former can realize the passive cancellation of scattered electromagnetic waves by arranging two frequency selective surfaces with a phase difference of 180° into a chessboard structure, the latter can receive the incident energy into the absorber structure through spatial impedance matching, and convert it into thermal energy through the structural or resistance loss, so as to reduce the scattering energy. The phase gradient surface (PGS) influences the propagation direction of scattering waves, which is used to reduce the monostatic RCS and control the peak of bistatic RCS [10]. The polarization conversion metasurface (PCM) can scatter electromagnetic waves that are orthogonal to the polarization of incident electromagnetic waves. Besides, the PCM can be arranged as a checkerboard to realize RCS reduction [11]–[14].

The Fabry-Perot antenna (FPA) is the integrated design of antennas and metamaterials. The partial reflective surface (PRS) is used to improve the gain of the source antenna, usually a microstrip antenna. The PRS with positive reflection phase gradient can widen the gain bandwidth of the FPA [15]. By introducing the idea of phase-modulated metasurface into the design of the PRS, the beam steering of the FPA can be realized [16]–[18]. In addition, the FPA can realize partly the balance of radiation and scattering performance of

antennas [19]–[29]. On the one hand, the cavity composed of the PRS and reflector causes the multiple reflections of the electromagnetic waves radiated by the source antenna, which ensures the out waves in phase. On the other hand, the FPA has a good in-band scattering performance due to multiple losses in the cavity. Furthermore, metamaterials can be used to reduce the RCS outside the operating band of the FPA, thus reducing the RCS within a wide band and ensuring the stability of radiation performance. The MA replaces the metal reflector of the FPA to further improve the in-band RCS reduction, but the high gain characteristics is lost [19]. A coding metasurface is designed in the upper layer of the PRS, which realizes a broadband RCS reduction but slightly deviates the main beam direction [20]. The combination of the MA and PRS can reduce the RCS out of band and weaken the influence on the gain of the FPA [21]–[23]. The FSS and PCM are arranged as checkerboard metasurface (CM) as the upper layer of the PRS, a broadband RCS reduction can also be realized [24]–[29]. Both the PGS and MA are used to design the PRS, the PGS improve the in-band RCS and the MA reduce the RCS within a wide band [30]. In most researches, the reference antenna for RCS reduction is the microstrip antenna, which are not directly compared with FPA. In fact, the in-band RCS is more complicated than the RCS out of band, especially the AM-RCS exists in the band. The AM-RCS is not ignored under the condition that the SM-RCS can be comparable to AM-RCS for a low RCS antenna. The reflection magnitude and phase of the antenna loads have a great effect on the AM-RCS, so the radio circuit matching technology is the main method to suppress the AM-RCS of antennas. The circulator and phase shifter are terminated on the ports of an antenna array [31], [32], and the AM-RCS would be manipulated to cancel out the SM-RCS, but it requires the circulator and phase shifter with a high-level impedance matching performance.

Different from the references, the AM-RCS is eliminated directly by the matched load. The RCS of a low RCS antenna is further reduced by manipulating AM-RCS in this article. The minimum RCS can be realized when the AM-RCS and SM-RCS with the equal amplitude and phase difference of 180 degrees. In this work, a method to reduce the in-band RCS of FPA is proposed based on the cancellation between the AM-RCS and SM-RCS. The transmitting and receiving microstrip antenna arrays are connected by metallized via to form the PRS of the proposed high-gain FPA. The RCS of the proposed FPA terminated with a special load is divided into the SM-RCS and AM-RCS. The feed line length of the FPA is adjusted to providing the phase difference of 180 degrees between the AM-RCS and SM-RCS at the center frequency. The impedance bandwidth of the proposed antenna is 9.8-11.2 GHz and the gain loss of the proposed antenna is 1.9 dB due to the addition of the phase delay line (PDL). The measured minimum monostatic RCS of proposed FPA terminated with open load reaches −32.7 dBsm, which is 17.9 dB lower than that of the reference FPA. At the center frequency, the bistatic RCS of the FPA terminated with
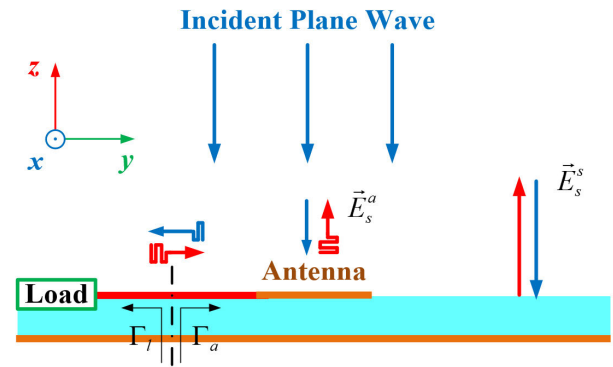

FIGURE 1. Schematic diagram of antennas scattering field.

open load is less than −14 dBsm within ±90 degrees angle domain, and especially it is less than −30 dBsm within ±8.7 degrees angle domain. Furthermore, this article provides the constraint condition for the feed line length of the FPA from the perspective of scattering performance.

II. THEORY OF DIVIDING SCATTERING FIELD

Assumed a linearly polarized plane wave is incident on a broadside antenna placed on the *x-y* plane, the schematic diagram of antenna scattering field is shown by Fig. 1. As we all know, the antennas need to be terminated with radio frequency (RF) devices such as amplifiers, filters, receivers, and so on. In fact, the RF-devices are regard as the load of the antennas, and they can not match with the antennas perfectly. Therefore, part of the energy received by the antenna is reflected by the load of the antenna, which excites the antenna again to produce a secondary radiation field in the space. The secondary radiation field is called the antenna mode scattering field (AM-SF), and the remainder of total scattering field (SF) removed to the AM-SF is the structural mode scattering field (SM-SF). Considering the relationship between the RCS and scattering field, the antenna RCS is composed of the AM-RCS and SM-RCS. The total scattering electric field $\vec{\mathbf{E}}_s$ of antennas is the vector superposition of the AM-SF and SM-SF [1].

$$\vec{\mathbf{E}}_s = \vec{\mathbf{E}}_s^s + \vec{\mathbf{E}}_a^s = \vec{\mathbf{E}}_s^s + \frac{\Gamma_l}{1 - \Gamma_l \Gamma_a} \vec{\mathbf{E}}_1^t b_0^m \quad (1)$$

where $\vec{\mathbf{E}}_s^s$ and $\vec{\mathbf{E}}_a^s$ are the SM-SF and AM-SF respectively, $\vec{\mathbf{E}}_1^t$ is electric field radiated by the antenna excited by a unit source, b_0^m is the magnitude of the receiving electric field for the antenna with matched load, Γ_l and Γ_a are the reflection coefficient of load and antenna respectively. The $\vec{\mathbf{E}}_a^s$ is related to the load and radiation field of antennas, so it matters for the high-gain antenna.

Based on the definition of AM-SF and SM-SF, the AM-SF disappears when the antenna is terminated with the matched load, and the total scattering field is equal to the SM-SF. However, the ideal matched load is difficult to achieve in practical engineering, so the method to divide the SF is proposed based on antennas terminated with two loads as following. Considering that the SM-SF independent of the loads, the SF can be divided into the SM-SF and AM-SF
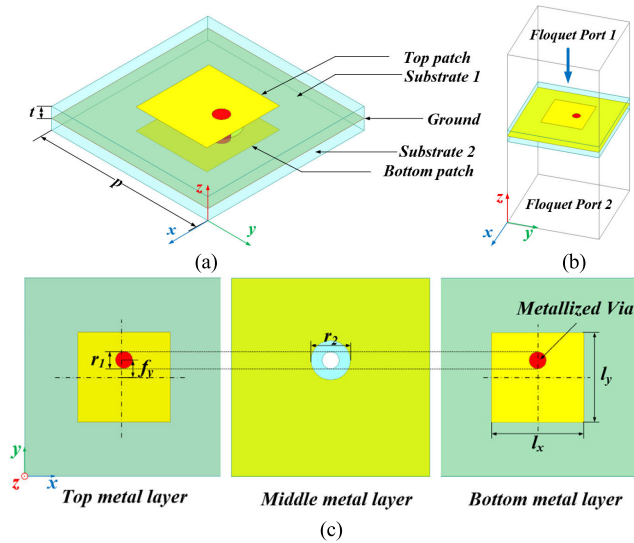
FIGURE 2. Element of the partial reflective surface. (a) 3-D structure. (b) Simulated model. (c) Top view.

by calculating the total scattering electric field of antenna terminated with different loads twice,

$$\vec{E}_s^1 = \vec{E}_s^s + \frac{\Gamma_l^1}{1 - \Gamma_l^1 \Gamma_a} \vec{E}_1^t b_0^m$$

$$\vec{E}_s^2 = \vec{E}_s^s + \frac{\Gamma_l^2}{1 - \Gamma_l^2 \Gamma_a} \vec{E}_1^t b_0^m \qquad (2)$$

The AM-SF of the antenna with the load reflection cofficient Γ_l^0 is

$$\vec{E}_a^s = \frac{\Gamma_l^0}{1 - \Gamma_l^0 \Gamma_a} \left(\vec{E}_s^1 - \vec{E}_s^2 \right) \Big/ \left(\frac{\Gamma_l^1}{1 - \Gamma_l^1 \Gamma_a} - \frac{\Gamma_l^2}{1 - \Gamma_l^2 \Gamma_a} \right) \qquad (3)$$

Without loss of generality, the open load and short load can be used to divide scattering field. The AM-SF is affected by the load, and the minimum RCS can be achieved by subtracting the AM-RCS from the SM-RCS.

III. DESIGN AND ANALYSIS OF THE ANTENNA

A. DESIGN OF THE PARTIAL REFLECTIVE SURFACE
The element of the PRS is illustrated by Fig. 2. The model is simulated by the infinite periodic boundary in Ansys HFSS. The patch antenna is terminated with another exactly the same patch antenna. The bottom antenna is the matched load of the top one. The energy received by the top antenna is transmitted to the bottom antenna, so the original AM-SF excitation source of the top antenna has become the radiation excitation source of the bottom antenna. The stacked antenna with metallic via is the element of the PRS, the period of element is fixed as $p = 15$ mm. All the dielectric substrates are FR4_epoxy with the thickness of 1 mm ($\varepsilon_r = 4.4$ and tan $\delta = 0.02$). The linearly polarized microstrip patch antenna resonates at 10 GHz, so the size of patch can be determined as $l_x = 7$ mm, $l_y = 6.8$ mm, and $f_y = 1.3$ mm. The radius of metallized via is $r_1 = 0.65$ mm, and there is a
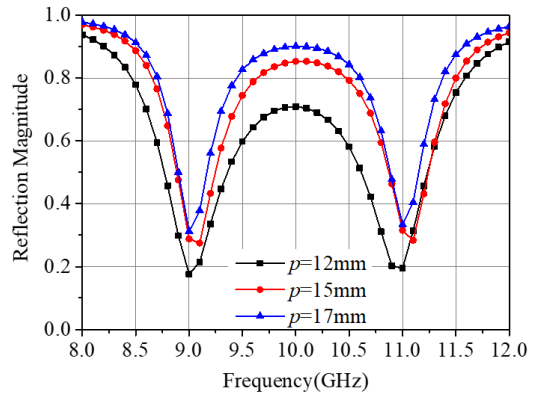

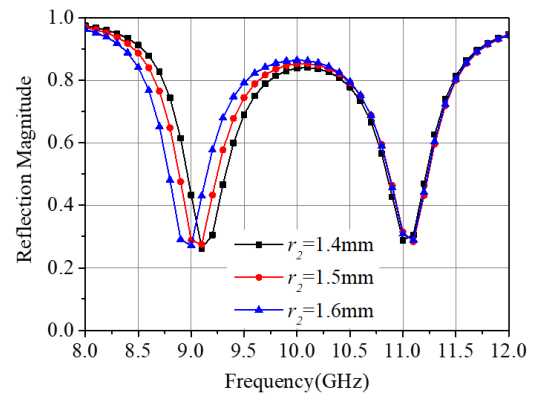FIGURE 3. Simulated reflection magnitude of the element with the change of p.

FIGURE 4. Simulated reflection magnitude of the element with the change of r_2.

circular slot with radius of $r_2 = 1.5$ mm in the middle metal ground. Viewed from the top or bottom, the element is the y polarized microstrip antenna, so the element is transparent to the co-polarized electromagnetic waves but reflects the cross-polarized ones. The parameters p and r_2 are optimized so that the reflectivity R of the element is larger enough. The relationship between the directivity and reflectivity of PRS is

$$D = 10 \lg \frac{1 + R}{1 - R} \qquad (4)$$

where D represents the theoretical maximum directivity of the FPA excited by source antenna with 0 dBi. Fig. 3 and Fig. 4 depict the simulated reflection magnitude of the element with the change of p and r_2. When p increases to 17 mm, the reflection magnitude reaches 0.9, whereas the period of element is larger than half wavelength of 10 GHz, which would raise the sidelobe level. The larger the parameter r_2 is, the higher the reflection magnitude is, but it would cause the resonate frequency to move down. The final parameters are shown in Table 1. Fig. 5 describes the simulated co-polarized and cross-polarized reflection coefficient of the element. The co-polarized reflection magnitude and phase are 0.85 and 187.7 degrees respectively at 10 GHz. The cross-polarized reflection magnitude and phase are 0.71 and 231 degrees respectively at 10 GHz.

TABLE 1. Parameters of the element.

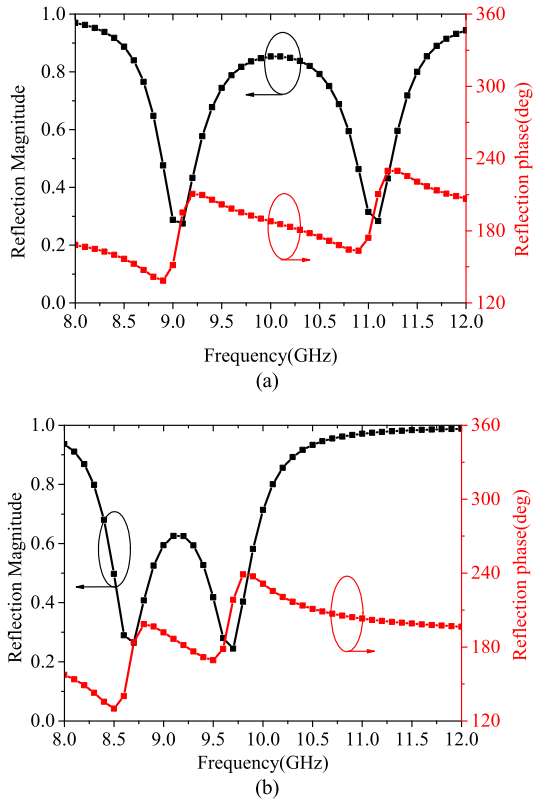| parameters	p	r_1	r_2	l_x	l_y	f_y	t
value(mm)	15	0.65	1.5	7	6.8	1.3	1

FIGURE 5. Simulated (a) co-polarization and (b) cross-polarization reflection coefficient of the element.

The co-polarized reflection coefficient of the element is used to determine the height of Fabry-Perot cavity.

B. DESIGN OF THE FABRY-PEROT ANTENNA

The FPA belongs to a leaky wave antenna. Some of the electromagnetic waves radiated firstly by a source antenna are reflected in the Fabry-Perot cavity, and part of energy would be emitted through the PRS. By optimizing the cavity height, the electromagnetic waves leaked from the PRS would keep in phase to realize the high-gain FPA. In this case, the theoretical maximum directivity of the FPA excited by 0 dBi source antenna is 10.9 dBi. The cavity height is determined by the resonate condition,

$$\varphi_{up} + \varphi_{down} - 4\pi h / \lambda_c = 2N\pi, \quad N = 0, \pm 1, \pm 2 \quad (5)$$

where φ_{up} and φ_{down} are the phases of the PRS and reflector respectively. λ_c is the wavelength at the center frequency, h represents the height of Fabry-Perot cavity. N is generally selected as 0 to maintain the low profile of the FPA.

The simulation model of the FPA is shown in Fig. 6(a). The PRS consisting of 25 elements with dimensions 75 mm ×75 mm is designed. A microstrip antenna fed by side is used as the source antenna of the FPA, as shown in Fig. 6(b). The dielectric substrate of the source antenna is
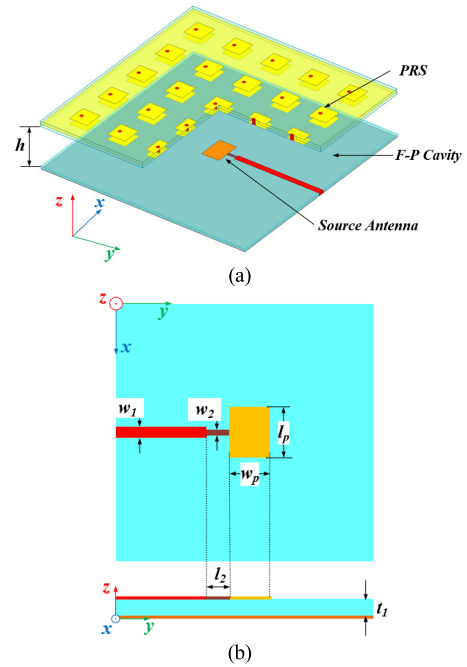

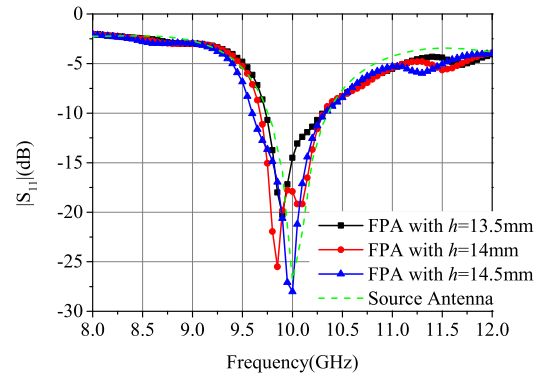**FIGURE 6.** Simulation model of (a) the FPA and (b) source antenna.

FIGURE 7. Simulated |S_{11}| with change of h.

FR4_epoxy with thickness $t_1 = 1$ mm, and the parameters of the source antenna are: $l_p = 9.4$ mm, $w_p = 6.6$ mm, $w_1 = 0.8$ mm, $w_2 = 2.1$ mm, $l_2 = 3.3$ mm. The substrate grounded is regarded as the bottom of the Fabry-Perot cavity, and its magnitude and phase φ_{down} are 1 and 154.7 degrees respectively. In this case, the height of the FPA is $h = 13.9$ mm, calculated by equation (5). However, there is always a deviation between theory and practice, the cavity height h needs to be optimized in order to reach the maximum broadside directivity at 10 GHz.

Fig. 7 describes the simulated reflection magnitude with change of h. The PRS can slightly broaden the bandwidth of source antenna, and the operating bandwidth of the FPA increases from 5.7% to 7.4% as h increases from 13.5mm to 14.5 mm. Fig. 8 demonstrates the directivity with change of h. When h increases from 13.5 mm to 14.5 mm, the maximum directivity of the FPA increases and then decreases, and the frequency corresponding to the maximum directivity also shifts. The maximum directivity 16.4 dBi is obtained
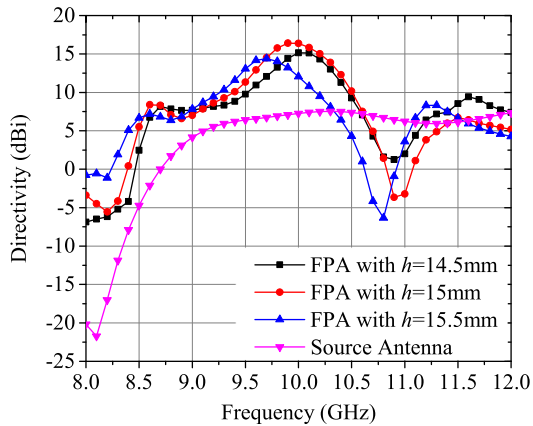
FIGURE 8. Simulated directivity with change of *h*.

at the center frequency when *h* is equal to 14 mm. The maximum directivity of FPA is 9.2 dB higher than that of source of the antenna. However, the increase value of the maximum directivity doesn't reach 10.9 dB, it may contribute to the finite size of the FPA and the loss of dielectric substrate.

C. ANALYSIS OF SCATTERING PERFORMANCE

The total RCS contains the SM-RCS and AM-RCS. The former is the RCS of the antenna terminated with matched load, and the latter originates from the reradiation fields of reflected energy in the antenna port. The AM-RCS is positively correlated with antenna gain, so it needs to be more concern for high gain antenna than others.

Fig. 9 demonstrates the simulated monostatic RCS of the FPA under normal incidence of plane waves with *x* and *y* polarization. The RCS curves in Fig. 9 (a) are close to coincide, so there is hardly the *x* polarized AM-RCS. Fig. 9 (b) shows that the *y* polarized RCS on short state is 4.7 dB higher than that on the open state at 10 GHz, which attributes to the AM-RCS. The bistatic RCS at 10 GHz is drawn in Fig. 10 to analyze the distribution of scattering energy. Fig. 10 (a) demonstrates that *x* polarized bistatic RCS is almost independent on the load. Fig. 10 (b) indicates the *y* polarized RCS is greatly affected by the load of the FPA, the RCS on the short state at 10 GHz is 4.7 dB higher than that on the matched state. In the end-fire direction, the RCS in the open state is larger than that in the matched state, and the difference between them is provided by the AM-RCS. Therefore, as a *y* polarized antenna, the AM-RCS of the FPA can be ignored under the incident wave with *x* polarization, while it deserves the attention for *y* polarization.

In order to accurately analyze the RCS of the FPA, the RCS is divided into the AM-RCS and SM-RCS based on equation (3). The RCS of the FPA is simulated by being terminated with 50 Ω, 30000 Ω and 0.0001 Ω loads as the matched, open and short loads respectively. The RCS components of the FPA under normal incidence with the *y* polarized plane wave are depicted in Fig. 11. The magnitude and phase of the SM-RCS are always the same, since they are independent on the load states. The magnitude of the AM-RCS should be the same
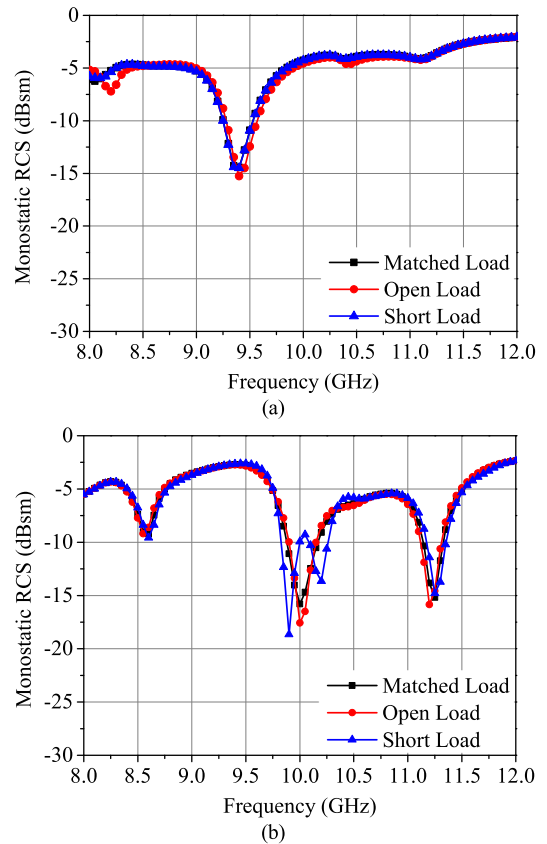

FIGURE 9. Simulated monostatic RCS of the FPA under normal incidence of plane waves with (a) *x* and (b) *y* polarization.

for the FPA terminated with loads with the same reflection magnitude, and the magnitude difference in Fig. 11 (a) may be caused by the nonideal loads and the mesh difference between the two simulations. At 10 GHz, the AM-RCS magnitudes of the FPA terminated with open and short loads are −13.9 dBsm and −14.8 dBsm respectively, and the SM-RCS magnitude of the FPA is −16.1 dBsm. Fig. 11(b) indicates the phase of the RCS components on the open and short states. The phases of the AM-RCS terminated with the open and short load are are 124 degrees and 291 degrees respectively, and the SM-RCS phase of the FPA is 252 degrees. As shown in Fig. 11(c). The phase differences between the AM-RCS and SM-RCS on the open and short states are 231 degrees and 38 degrees at 10 GHz respectively. In order to reduce the RCS of the FPA, a special load should be selected to equalize the magnitudes of the AM-RCS and SM-RCS, and the microstrip feed line should be improved to realize the phase difference of 180 degrees between the two RCS components.

The load can be chosen to be close to the open load, considering that the maximum magnitude of AM-RCS is close to that of SM-RCS. The phase difference between the AM-RCS and SM-RCS is provided by the microstrip feed line except for the load. The field that a plane wave is received by the antenna and then reradiated is the AM-SF, so the excitation signal of the AM-SF needs to pass through the feed line twice. Therefore, the phase of the AM-RCS can be controlled by the microstrip phase delay line (PDL) and the
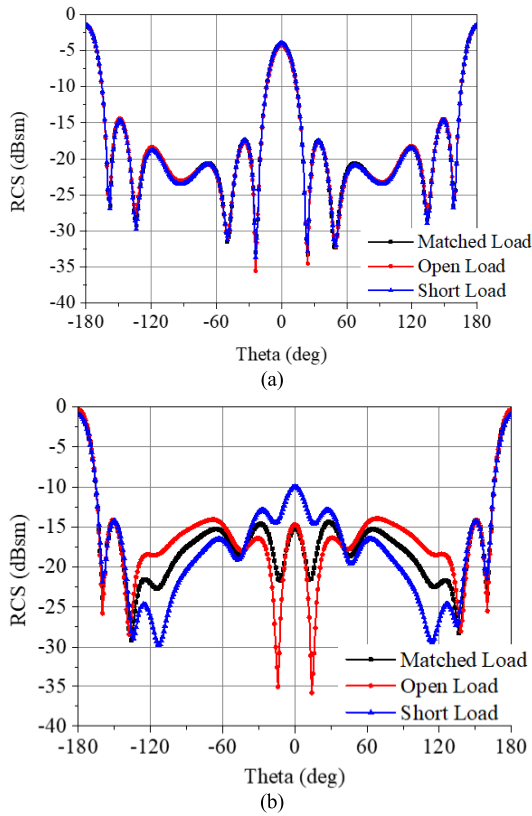
FIGURE 10. Simulated bistatic RCS of the FPA under normal incidence of plane waves with (a) *x* and (b) *y* polarization at 10GHz.

length l_o of the PDL is determined by

$$|\varphi_a - \varphi_s| + \varphi_o = |\varphi_a - \varphi_s| + 2kl_o = 180n,$$
$$n = \pm 1, \pm 3, \pm 5 \dots \qquad (6)$$

where φ_a and φ_s are the phase of the AM-RCS and SM-RCS respectively, φ_o is the phase of the PDL, k is the effective propagation constant in the dielectric substrate, n is selected based on the principle of the shortest phase delay line. The length of the PDL to realize 180 degrees phase difference between the AM-RCS and SM-RCS is

$$l_o = (7.1n - 9.2) \text{ mm}, \quad n = 1, 3, 5 \dots \qquad (7)$$

The simulation model of the proposed FPA is shown in Fig. 12. The length of the PDL is $l_o = 11.1$ mm according to equation (7) when $n = 3$. The final length of the PDL is optimized to 9.4 mm to minimize the total RCS of the FPA. Fig 13 describes the simulated monostatic RCS of the FPA terminated with open load under normal incidence with *y* polarized plane wave. Compared with the reference FPA without PDL, the monostatic RCS of the proposed FPA with PDL is reduced remarkably from -13.9 dBsm to -33.5 dBsm at 10 GHz, but the RCS of the proposed FPA is higher than that of the reference one at some frequencies in the operating band since the phase of the PDL is frequency sensitive. The monostatic RCS curves outside the operating band between the proposed and reference FPA are around coincide. The FPA can hardly receive energy outside the operating band, and the AM-RCS can be ignored.
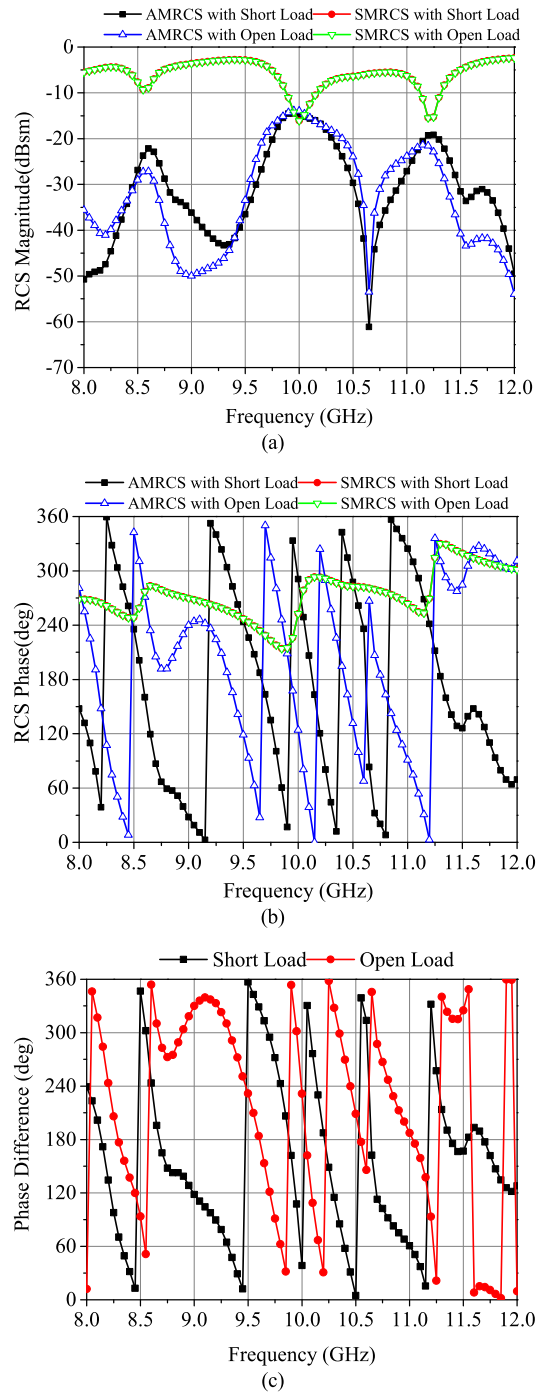

FIGURE 11. RCS components of the FPA under normal incidence with y polarized plane wave. (a) Magnitudes and (b) phases of RCS components, (c) phase differences between the AM-RCS and SM-RCS.

Fig. 14 shows the simulated bistatic RCS of the proposed FPA under normal incidence of plane waves with *x* and *y* polarization at 10 GHz. It is observed that the bistatic RCS of the FPA is less than -14.1 dBsm in the upper half domain, especially it is less than -30 dBsm within ± 8.7 degrees. Compared with the source antenna, FPA realizes a certain RCS reduction, and the in-band RCS of FPA can be further reduced by controlling the AM-RCS. The simulated realized gain of the FPA is depicted in Fig. 15. The frequency
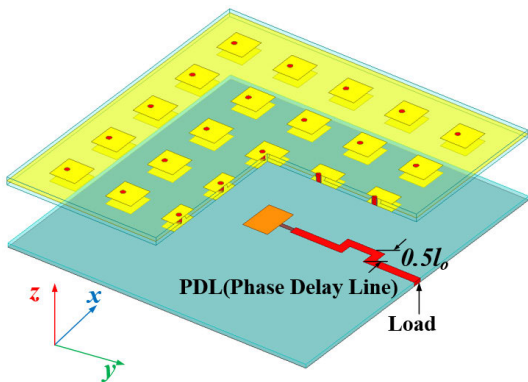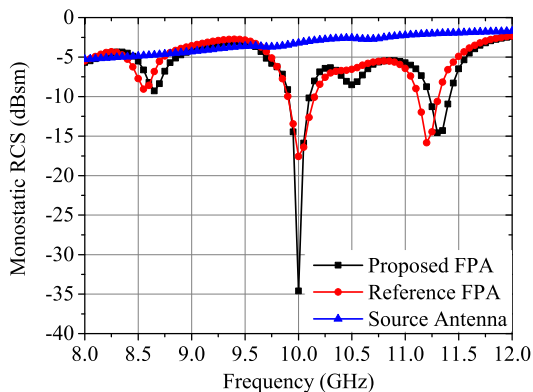
FIGURE 12. Simulation model of the proposed FPA.

FIGURE 13. Simulated monostatic RCS of the FPA terminated with open load under normal incidence with *y* polarized plane wave.
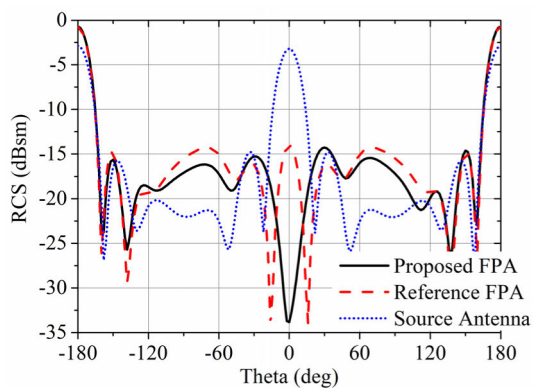

FIGURE 14. Simulated bistatic RCS of the FPA terminated with open load under normally incidence with *y* polarization.
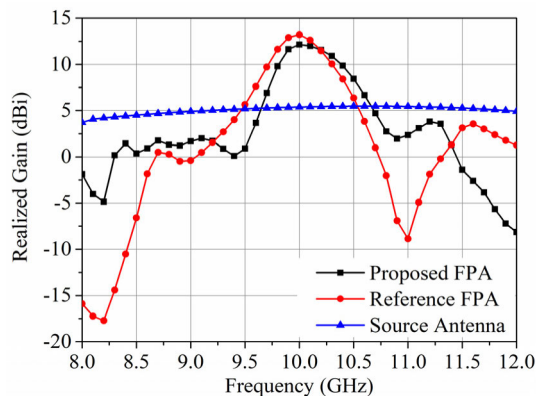

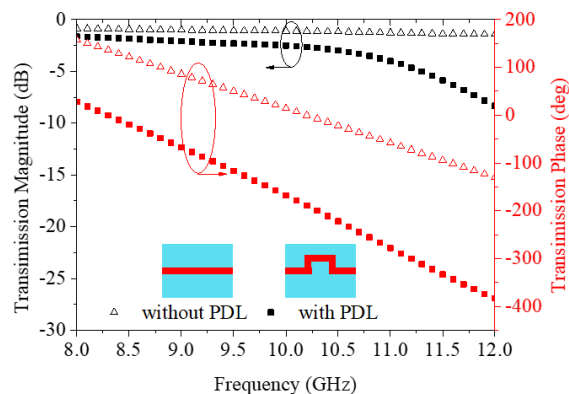**FIGURE 15.** Simulated realized gain of the FPA.

FIGURE 16. Transmission coefficient of the microstrip lines with or without the PDL.

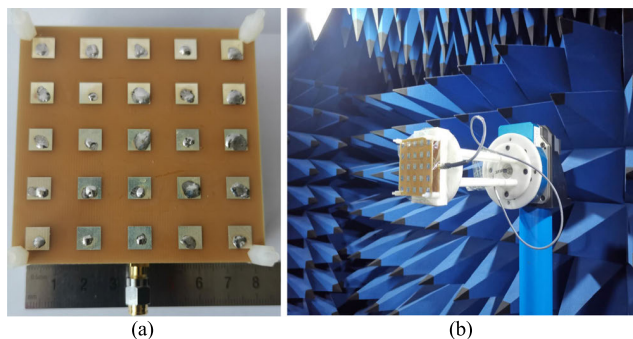**FIGURE 17.** (a) Fabricated prototype of the proposed FPA terminated with open load. (b) Fabricated FPA in an anechoic chamber.

getting the maximum gain remains unchanged, but the gain is reduced by 1.9 dB at 10 GHz. The transmission coefficient of the microstrip feed line is shown in Fig. 16. At 10 GHz, the insertion loss of the PDL is around 1.2 dB, and the phase difference between the two lines is $\varphi_o = 215$ degrees. The gain loss of the proposed FPA is mainly caused by the PDL, and it is inevitable but can be improved by using the low lossy dielectric substrate.

IV. MEASURED RESULTS DISCUSSION
In order to verify the proposed reduction technology of in-band RCS of the high gain FPA, a 75 mm × 75 mm × 17 mm FPA is manufactured in this article, and the length of

the PDL is 9.4 mm. Four nylon columns are used to support the cavity structure. The final fabricated prototype is shown in Fig. 17. The $|S_{11}|$ of the proposed FPA is measured by the Keysight N9952A FieldFox. Fig. 18 (a) describes the $|S_{11}|$ of the proposed FPA. The measured results show that the operating bandwidth of the proposed FPA is 1.4 GHz (from 9.8 GHz to 11.2 GHz). Fig. 18(b) demonstrates the realized gain of the proposed FPA. The maximum measured gain of the proposed FPA is 10.7 dBi at 10.2 GHz, which is 1.2dB less than the maximum simulated gain at 10 GHz.

The RCS of the proposed FPA terminated with the open load is measured. The schematic view of the RCS
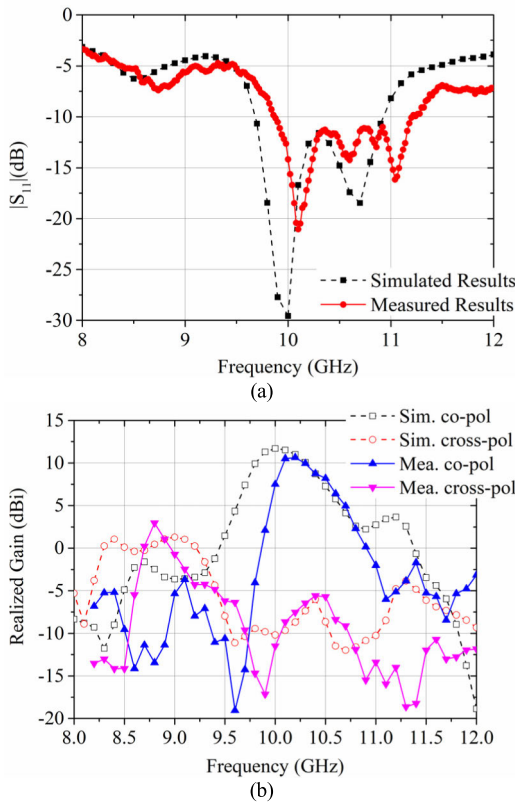
FIGURE 18. (a) Reflection magnitude and (b) realized gain vs. frequency of the proposed FPA.

FIGURE 19. Schematic view of the RCS measurement setup in an anechoic chamber.

FIGURE 20. Simulated and measured monostatic RCS of the FPA terminated with open load under normal incidence of plane waves with (a) *x* and (b) *y* polarization.

measurement setup is given in Fig. 19. The simulated and measured monostatic RCS of the FPA terminated with the open load under normal incidence of plane waves with *x* and *y* polarization are depicted in Fig. 20. When *x* polarized plane wave incident vertically to the proposed *y* polarized FPA, the monostatic RCS curve of the proposed FPA is shifted 0.1 GHz to the high frequency compared with the reference FPA.

When *y* polarized plane wave incident vertically to the FPA, the measured minimum monostatic RCS of the proposed FPA is −32.7 dBsm, which is 17.9 dB lower than simulated minimum monostatic RCS of the reference FPA (−14.8 dBsm). Compared with the simulated monostatic RCS curves, the trend of the measured results is consistent, but the overall curves move 0.2 GHz to the high frequency, which is caused by the inconsistency between the equivalent permittivity of substrate. After the simulation, the equivalent permittivity of FR4_epoxy used in actual processing is 4.1 instead of 4.4.

Table 2 represents the comparison of the maximum in-band RCS reduction between the designed antenna and existed work. It can be observed that the Fabry-Perot cavity combined with metamaterials are used to reduce the RCS of the source antenna (microstrip antenna), but few papers have proposed RCS reduction techniques directly compared with FPA. In addition, considering that the AM-RCS is eliminated by the FPA terminated with the matched load, the metamaterials only act on the SM-RCS. In this work, we propose
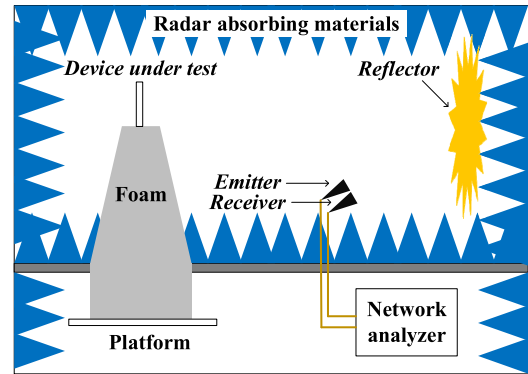
the PDL to reduce the FPA without metamaterials, and the AM-RCS is used to cancel out the AM-RCS instead of being eliminated by the matched load. This work provides a new idea for RCS reduction technology of antennas, and can be combined with other RCS reduction technologies to achieve more effective RCS reduction, which will be our next work.

The AM-RCS is the important component of an antenna RCS. Compared with eliminating the AM-RCS of an antenna and treating the antenna as a general scatterer, it is more meaningful to further reduce the RCS of the antenna by

TABLE 2. Comparison between the designed antenna and existed work.

Year/ Reference	10-dB impedance bandwidth	Maximum in-band RCS reduction				Metamaterials type for RCS reduction	Area (λ^2)	Termination load
		Reference antenna	RCS before being reduced	RCS after being reduced	RCS reduction			
2017/ [27]	9.2-10.1 GHz (8.8%)	Microstrip antenna	-17 dBsm	-37 dBsm	20 dB	PCM CM	1.25×1.25	Matched load
2018/ [25]	9.4-11.1 GHz (16.4%)	Microstrip antenna	-4.5 dBsm	-43.9 dBsm	39.4 dB	FSS CM	2.3×2.3	Matched load
2018/ [21]	10.5-10.8 GHz (1.8%)	Microstrip antenna	-4 dBsm	-30 dBsm	26 dB	MA	2.7×2.7	Matched load
2019/ [28]	9.5-12.8 GHz (29.5%)	Microstrip antenna	-4 dBsm	-24 dBsm	20 dB	PCM CM	3×3	Not mentioned
2019/ [26]	26.7-34.2 GHz (24.6%)	Microstrip antenna	0 dBsm	-15 dBsm	15 dB	FSS CM	5.1×5.1	Not mentioned
2019/ [30]	8.37-8.52 GHz (1.8%)	Microstrip antenna	2 dBsm	15 dBsm	13 dB	PGS	3.4×3.4	Not mentioned
2020/ [24]	8.5-12.2 GHz (36.1%)	Microstrip antenna	-2.8 dBsm	-24 dBsm	21.2 dB	PCM CM	2.7×2.7	Not mentioned
This work	9.8-11.2 GHz (13.3%)	Fabry-Peort antenna	-14.8 dBsm	-32.7 dBsm	17.9 dB	No Metamaterials	2.6×2.6	Open load

utilizing the AM-RCS. The RCS reduction of the antenna can be realized by optimizing the AM-RCS, and the value of reduction is related to the magnitude difference of the SM-RCS and the AM-RCS. This article provides a new idea for RCS reduction of antennas.

V. CONCLUSION

In this article, a high reflectivity PRS is proposed to design the high-gain FPA. The microstrip phase delay line is used to control the AM-RCS phase of the FPA. The in-band RCS of the low RCS high-gain FPA is further reduced based on the cancellation between AM-RCS and SM-RCS. The bandwidth of $|S_{11}| < -10$ dB is 9.8-11.2 GHz, and the maximum realized gain is 10.7 dBi at 10.2 GHz. The minimum mono-static RCS of proposed FPA terminated with open load is 17.9 dB lower than that of the reference FPA. The bistatic RCS of the FPA is less than -14 dBsm within ±90 degrees angle domain at center frequency. This article provides the constraint condition for the feed line length of FPA from the perspective of scattering performance, and a new idea for RCS reduction technology of antennas.

REFERENCES

[1] R. C. Hansen, "Relationships between antennas as scatterers and as radiators," *Proc. IEEE*, vol. 77, no. 5, pp. 659–662, May 1989.

[2] W. Jiang, Y. Liu, S. Gong, and T. Hong, "Application of bionics in antenna radar cross section reduction," *IEEE Antennas Wireless Propag. Lett.*, vol. 8, pp. 1275–1278, 2009.

[3] D. Colak, A. I. Nosich, and A. Altintas, "Radar cross-section study of cylindrical cavity-backed apertures with outer or inner material coating: The case of E-polarization," *IEEE Trans. Antennas Propag.*, vol. 41, no. 11, pp. 1551–1559, Nov. 1993.

[4] M. Pazokian, N. Komjani, and M. Karimipour, "Broadband RCS reduction of microstrip antenna using coding frequency selective surface," *IEEE Antennas Wireless Propag. Lett.*, vol. 17, no. 8, pp. 1382–1385, Aug. 2018.

[5] Y. Liu, Y. Hao, H. Wang, K. Li, and S. Gong, "Low RCS microstrip patch antenna using frequency-selective surface and microstrip resonator," *IEEE Antennas Wireless Propag. Lett.*, vol. 14, pp. 1290–1293, 2015.

[6] A. Sharma, B. K. Kanaujia, S. Dwari, D. Gangwar, S. Kumar, H. C. Choi, and K. W. Kim, "Wideband high-gain circularly-polarized low RCS dipole antenna with a frequency selective surface," *IEEE Access*, vol. 7, pp. 156592–156602, 2019.

[7] S. Genovesi, F. Costa, and A. Monorchio, "Wideband radar cross section reduction of slot antennas arrays," *IEEE Trans. Antennas Propag.*, vol. 62, no. 1, pp. 163–173, Jan. 2014.

[8] Y. Liu and X. Zhao, "Perfect absorber metamaterial for designing low-RCS patch antenna," *IEEE Antennas Wireless Propag. Lett.*, vol. 13, pp. 1473–1476, 2014.

[9] K. Payne, K. Xu, J. H. Choi, and J. K. Lee, "Electrically tunable microwave absorber based on discrete plasma-shells," *IEEE Trans. Antennas Propag.*, vol. 67, no. 10, pp. 6523–6531, Oct. 2019.

[10] W. Zhang, Y. Liu, S. Gong, J. Wang, and Y. Jiang, "Wideband RCS reduction of a slot array antenna using phase gradient metasurface," *IEEE Antennas Wireless Propag. Lett.*, vol. 17, no. 12, pp. 2193–2197, Dec. 2018.

[11] Y. Jia, Y. Liu, Y. J. Guo, K. Li, and S.-X. Gong, "Broadband polarization rotation reflective surfaces and their applications to RCS reduction," *IEEE Trans. Antennas Propag.*, vol. 64, no. 1, pp. 179–188, Jan. 2016.

[12] Y. Lu, J. Su, J. Liu, Q. Guo, H. Yin, Z. Li, and J. Song, "Ultrawideband monostatic and bistatic RCS reductions for both copolarization and cross polarization based on polarization conversion and destructive interference," *IEEE Trans. Antennas Propag.*, vol. 67, no. 7, pp. 4936–4941, Jul. 2019.

[13] S. Sun, W. Jiang, X. Li, P. Liu, and S. Gong, "Ultrawideband high-efficiency 2.5-dimensional polarization conversion metasurface and its application in RCS reduction of antenna," *IEEE Antennas Wireless Propag. Lett.*, vol. 18, no. 5, pp. 881–885, May 2019.

[14] S. Sun, W. Jiang, S. Gong, and T. Hong, "Reconfigurable Linear-to-Linear polarization conversion metasurface based on PIN diodes," *IEEE Antennas Wireless Propag. Lett.*, vol. 17, no. 9, pp. 1722–1726, Sep. 2018.

[15] N. Wang, Q. Liu, C. Wu, L. Talbi, Q. Zeng, and J. Xu, "Wideband Fabry–Pérot resonator antenna with two complementary FSS layers," *IEEE Trans. Antennas Propag.*, vol. 62, no. 5, pp. 2463–2471, May 2014.

[16] A. Ghasemi, S. N. Burokur, A. Dhouibi, and A. de Lustrac, "High beam steering in Fabry–Pérot leaky-wave antennas," *IEEE Antennas Wireless Propag. Lett.*, vol. 12, pp. 261–264, 2013.

[17] S. N. Burokur, J.-P. Daniel, P. Ratajczak, and A. de Lustrac, "Tunable bilayered metasurface for frequency reconfigurable directive emissions," *Appl. Phys. Lett.*, vol. 97, no. 6, Aug. 2010, Art. no. 064101.

[18] B. Ratni, W. A. Merzouk, A. de Lustrac, S. Villers, G.-P. Piau, and S. N. Burokur, "Design of phase-modulated metasurfaces for beam steering in Fabry–Pérot cavity antennas," *IEEE Antennas Wireless Propag. Lett.*, vol. 16, pp. 1401–1404, 2017.

[19] J. Mu, H. Wang, H. Wang, and Y. Huang, "Low-RCS and gain enhancement design of a novel partially reflecting and absorbing surface antenna," *IEEE Antennas Wireless Propag. Lett.*, vol. 16, pp. 1903–1906, 2017.

[20] L. Zhang, X. Wan, S. Liu, J. Y. Yin, Q. Zhang, H. T. Wu, and T. J. Cui, "Realization of low scattering for a high-gain Fabry–Pérot antenna using coding metasurface," *IEEE Trans. Antennas Propag.*, vol. 65, no. 7, pp. 3374–3383, Jul. 2017.

[21] J. Ren, W. Jiang, K. Zhang, and S. Gong, "A high-gain circularly polarized Fabry–Pérot antenna with wideband low-RCS property," *IEEE Antennas Wireless Propag. Lett.*, vol. 17, no. 5, pp. 853–856, May 2018.

[22] W. Pan, C. Huang, P. Chen, X. Ma, C. Hu, and X. Luo, "A low-RCS and high-gain partially reflecting surface antenna," *IEEE Trans. Antennas Propag.*, vol. 62, no. 2, pp. 945–949, Feb. 2014.

[23] C. Huang, W. Pan, X. Ma, and X. Luo, "A frequency reconfigurable directive antenna with wideband low-RCS property," *IEEE Trans. Antennas Propag.*, vol. 64, no. 3, pp. 1173–1178, Mar. 2016.

[24] Z. Liu, S. Liu, J. Bornemann, X. Zhao, X. Kong, Z. Huang, B. Bian, and D. Wang, "A low-RCS, high-GBP Fabry–Pérot antenna with embedded chessboard polarization conversion metasurface," *IEEE Access*, vol. 8, pp. 80183–80194, 2020.

[25] Y. Zheng, J. Gao, Y. Zhou, X. Cao, H. Yang, S. Li, and T. Li, "Wideband gain enhancement and RCS reduction of Fabry–Pérot resonator antenna with chessboard arranged metamaterial superstrate," *IEEE Trans. Antennas Propag.*, vol. 66, no. 2, pp. 590–599, Feb. 2018.

[26] S. Zarbakhsh, M. Akbari, F. Samadi, and A.-R. Sebak, "Broadband and high-gain circularly-polarized antenna with low RCS," *IEEE Trans. Antennas Propag.*, vol. 67, no. 1, pp. 16–23, Jan. 2019.

[27] M. Long, W. Jiang, and S. Gong, "Wideband RCS reduction using polarization conversion metasurface and partially reflecting surface," *IEEE Antennas Wireless Propag. Lett.*, vol. 16, pp. 2534–2537, 2017.

[28] Q. Chen and H. Zhang, "High-gain circularly polarized Fabry–Pérot patch array antenna with wideband low-radar-cross-section property," *IEEE Access*, vol. 7, pp. 8885–8889, 2019.

[29] Y. Liu, Y. Jia, W. Zhang, and F. Li, "Wideband RCS reduction of a slot array antenna using a hybrid metasurface," *IEEE Trans. Antennas Propag.*, vol. 68, no. 5, pp. 3644–3652, May 2020.

[30] Y. Jia, Y. Liu, W. Zhang, J. Wang, S. Gong, and G. Liao, "High-gain Fabry–Pérot antennas with wideband low monostatic RCS using phase gradient metasurface," *IEEE Access*, vol. 7, pp. 4816–4824, 2019.

[31] N. Nakamoto, T. Takahashi, T. Fukasawa, and N. Yoneda, "RCS reduction of array antenna using circulator and phase shifter," in *Proc. IEEE Conf. Antenna Meas. Appl. (CAMA)*, Tsukuba, Japan, Dec. 2017, pp. 190–193.

[32] N. Nakamoto, T. Takahashi, T. Nomura, M. Otsuka, and H. Miyashita, "A method to measure the antenna mode and structural mode for antenna RCS reduction using circulator and phase shifter," in *Proc. Int. Symp. Antennas Propag. Conf.*, Kaohsiung, Japan, Dec. 2014, pp. 21–22.
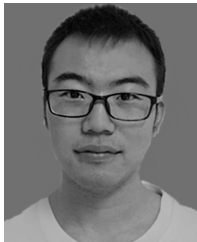
QIANG CHEN (Senior Member, IEEE) received the B.E. degree from Xidian University, Xi'an, China, in 1986, and the M.E. and D.E. degrees from Tohoku University, Sendai, Japan, in 1991 and 1994, respectively.

He is currently an Associate Professor with the Department of Electrical Communications, Tohoku University. His primary research interests include computational electromagnetics, array antennas, and antenna measurement.

Dr. Chen is a member of IEICE. He received the Young Scientists Award in 1993, the Best Paper Award and Zen-ichi Kiyasu Award, in 2009 from the Institute of Electronics, Information, and Communication Engineers (IEICE) of Japan. He served as the Secretary and a Treasurer of the IEEE Antennas and Propagation Society Japan Chapter, in 1998, the Secretary of Technical Committee on Electromagnetic Compatibility of IEICE, from 2004 to 2006, the Secretary of Technical Committee on Antennas and Propagation of IEICE, from 2008 to 2010. He has been an Associate Editor of the *IEICE Transactions on Communications*, since 2007.

LEI GAN was born in Gansu, China, in April 1995. He received the bachelor's degree from Xidian University, where he is currently pursuing the Ph.D. degree in electrical science and technology. His research interests include antenna scattering theory, antenna radar cross-section reduction, and phased array.

WEN JIANG (Member, IEEE) was born in Shandong, China, in November 1985. He received the bachelor's and Ph.D. degrees from Xidian University, Xi'an, China, in 2008 and 2012, respectively. He is currently the Vice Director with the National Key Laboratory of Science and Technology on Antennas and Microwaves, Xidian University, where he is also a Full Professor. His current research interests include electromagnetic scattering theory and technology, antenna theory and engineering, and electromagnetic measurement theory and technology.

XIAOQIU LI was born in Hunan, China. He received the Ph.D. degree in optics from the Graduate University of Chinese Academy of Science, in 2008. He is currently a Research Fellow with the Nanjing Research Institute of Electronics Technology. His research interests include electromagnetic scatters, phased antenna array, and frequency selective surface.

ZHIPENG ZHOU was born in 1967. He received the bachelor's degree in electromagnetic field and microwave technology from the University of Electronic Science and Technology of China, Chengdu, China, in 1989, and master's degree in engineering from the School of Optoelectronics, Nanjing University of Science and Technology, Nanjing, China, in 2004.

He is currently the Director of the Science and Technology on Antenna and Microwave Laboratory and the Chief Expert of the Nanjing Research Institute of Electronics Technology, Nanjing. In recent years, more than 40 academic articles and five books have been published. His main research interests include phased array antenna technology, microwave circuit design, and scattering suppression technology.

● ● ●